Research Article Vol. 3, No. 2 / 15 February 2020 / OSA Continuum 317

GaAs-based subwavelength grating on an AlO_x layer for a vertical-cavity surface-emitting laser

ANJIN LIU,[1,2,*] BO YANG,[1,2] PHILIP WOLF,[3] JING ZHANG,[1,2] AND DIETER BIMBERG[3,4]

[1] State Key Laboratory on Integrated Optoelectronics, Institute of Semiconductors, Chinese Academy of Sciences, Beijing 100083, China
[2] Center of Materials Science and Optoelectronics Engineering, University of Chinese Academy of Sciences, Beijing 100049, China
[3] Institute of Solid State Physics and Center of Nanophotonics, Technische Universität Berlin, Hardenbergstrasse 36, 10623 Berlin, Germany
[4] Bimberg Chinese-German Center for Green Photonics of the Chinese Academy of Sciences at CIOMP, Changchun, China
[*] liuanjin@semi.ac.cn

Abstract: A GaAs-based subwavelength grating on a thick (~3/4*λ at 1300 nm) AlO_x layer is designed, fabricated, and characterized. The AlO_x layer as a low-index medium is oxidized from a 640-nm $Al_{0.9}Ga_{0.1}As$ layer. The layer contraction of the $Al_{0.9}Ga_{0.1}As$ layer after wet oxidation to AlO_x is 4.9%. We fabricated GaAs-based subwavelength gratings on the AlO_x layer showing a high reflectivity of 90% in the 1300-nm wavelength range, consistent with the simulation results. Such GaAs-based subwavelength gratings can be used as high-contrast grating mirrors for narrow-linewidth VCSELs, improving the mechanical stability and simplifying the device fabrication.

1. Introduction

Vertical-cavity surface-emitting lasers (VCSELs) have broad applications in data communication, sensing, and consumer electronics. VCSELs have many advantages, such as circular beam, low power consumption, high modulation speed, low cost, high reliability, and easy fabrication of two-dimensional array configurations [1–4]. High-speed, energy-efficient, and temperature-stable VCSELs for data centers and high-performance computer systems, have made enormous progresses in recent years [3,4]. Recently high-efficiency VCSELs have also been developed for face recognition, flood illumination, and LiDAR [5,6]. Especially, VCSELs with a narrow linewidth are very promising laser sources for atomic magnetometer [7], coherent communication [8], and frequency standards [9], and have attracted much attention.

Typically, a VCSEL structure is composed of two distributed Bragg reflectors (DBRs), multiple quantum wells, and an oxide aperture for current and optical mode confinements. DBRs have a high reflectivity over a broad wavelength range because of multiple reflections with constructive interference among the waves reflected from different interfaces between high-index and low-index layers. Dozens of DBR layers are needed to achieve the required reflectivity being larger than 99.5% for the VCSEL application, making the VCSEL bulky. For DBR-based optoelectronic devices at blue-green or infrared wavelengths [10,11], it is not easy to grow DBRs.

Metastructures like high-index-contrast gratings (HCGs) have attracted much attention in the past few years [12–20]. A typical HCG has a thickness of a few hundreds of nanometers and has a nearly 100% reflectivity across a broad wavelength range [12], and can be used as a mirror in a VCSEL. HCG-VCSELs are now working at wavelengths of 850 nm [18], 980 nm [19,21], 1060 nm [22,23], and 1550 nm [24–26].

#384327 https://doi.org/10.1364/OSAC.384327
Journal © 2020 Received 26 Nov 2019; revised 18 Jan 2020; accepted 22 Jan 2020; published 3 Feb 2020

OSA CONTINUUM

The previously reported HCG-VCSELs always employ suspended subwavelength gratings surrounded by air to realize a high index contrast for mirrors. The fabrication of such suspended HCGs is complex because selective etching and grating release process are required. Suspended HCGs in addition suffer the problem of mechanical stability, and device lifetime might be shortened, because the low thermal conductivity of the air can negatively affect the overall performance of devices.

Some attempts have been made to realize HCG bars sitting on a low-index medium, without selective etching and a grating release process [27–29]. GaAs is a well researched material for VCSELs covering a wide wavelength range. GaAs-based HCGs with an AlO_x layer as the low-index medium are highly desirable for a mirror used in VCSELs. Almuneau *et al*. [27] used 150-nm AlAs to create AlO_x by wet oxidation as the low-index medium below a GaAs-based grating. This thickness of 150 nm was carefully chosen after considering the mechanical strain by the volume shrinkage of the AlAs layer.

The thickness of the low-index medium is an important parameter in HCG-VCSELs. A small thickness of the low-index medium can cause evanescent coupling between the HCG layer and the layer under the low-index medium, resulting in a low reflectivity of the part above the active region in the HCG-VCSEL. Thus, $5/4*\lambda$ and $1/2*\lambda$ air gaps were used for the HCG-VCSELs demonstrated in [18,19]. A thick ($1/2*\lambda$ and beyond) low-index medium like AlO_x is preferred to realize a long cavity in the HCG-VCSEL with a narrow linewidth [30]. Thus, when GaAs-based HCG bars are sitting on a thick AlO_x layer as the low-index medium, realization of such thick AlO_x layers is challenging.

In this work, we present a HCG based on GaAs/AlO_x layers. The HCG doesn't require selective etching and grating release process which are used in [18,19]. The subwavelength grating is defined on the GaAs layer on a 640-nm $Al_{0.9}Ga_{0.1}As$ layer oxidized to AlO_x ($n = 1.6$) with a layer contraction of 4.9%. The thickness of the low-index AlO_x layer is larger than the one in [27], and the HCG here has a better mechanical stability. The HCG shows a high reflectivity, consistent with the simulation results, and can be used as the mirror in narrow-linewidth VCSELs.

2. Design and fabrication

The Aluminum content and thickness of an AlGaAs layer affect the oxidation rate for given oxidation conditions. A high Aluminum content and a thick AlGaAs lead to a large oxidation rate [31]. There is a layer contraction of more than 6.7% for AlGaAs for an Aluminum content of 98% after wet oxidation, introducing considerable strain [32]. This strain may lead to layer delamination when the thickness of an $Al_{0.98}Ga_{0.02}As$ layer is too large. We tried a 600-nm $Al_{0.98}Ga_{0.02}As$ layer underneath the GaAs layer and layer delamination was observed. Thus, $Al_{0.9}Ga_{0.1}As$ layers for oxidation were adopted for less strain after wet oxidation.

The schematic and a scanning electron microscope (SEM) image of one of our HCGs are shown in Fig. 1. The grating period is Λ, and the width of the grating bar is a. The duty cycle (DC) is defined as a/Λ, and t_g is the thickness of the grating. The reflectivity contour of the HCG is calculated by the rigorous coupled wave analysis method. Results are shown in Fig. 2(a) for the normalized wavelength (λ/Λ) and the normalized thickness (t_g/Λ) of the grating for transverse magnetic polarization (TM, the electric field is perpendicular to the grating bar). The thickness and period of the HCGs are 362 nm and 560 nm, respectively.

Figure 2(b) shows the reflectivity contour of a HCG for a thickness of the AlO_x layer less than 1 μm. The reflectivity spectrum is periodically varying when the thickness of the AlO_x layer varies. When the thickness of the AlO_x layer is around 605 nm ($\sim 3/4*\lambda$), the reflectivity spectrum has its maximum bandwidth for a high reflectivity (more than 99.5%) for TM polarization. Considering the estimated layer contraction for the $Al_{0.9}Ga_{0.1}As$ layer after wet oxidation, the thickness of the $Al_{0.9}Ga_{0.1}As$ layer before oxidation is chosen to 640 nm. The HCG has a high reflectivity across the whole 1300-nm range.

OSA CONTINUUM

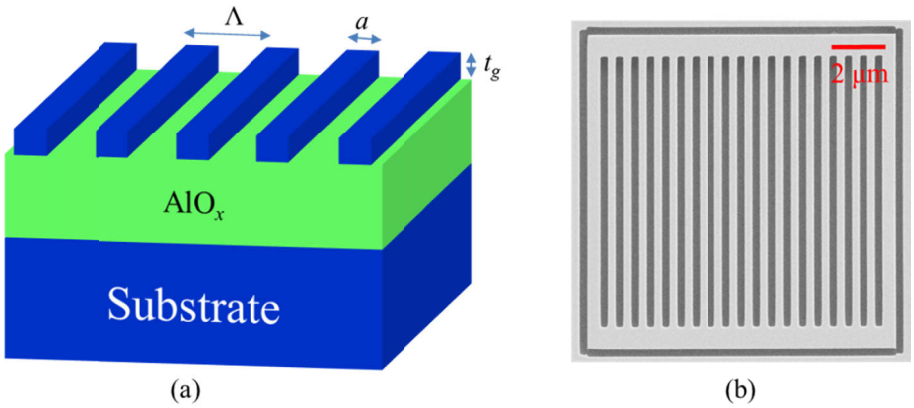

Fig. 1. (a) Schematic of the HCG. The grating period is Λ; a is the width of the grating bar; the duty cycle (DC) is defined as a/Λ; and t_g is the thickness of the grating. (b) SEM image of the HCG.

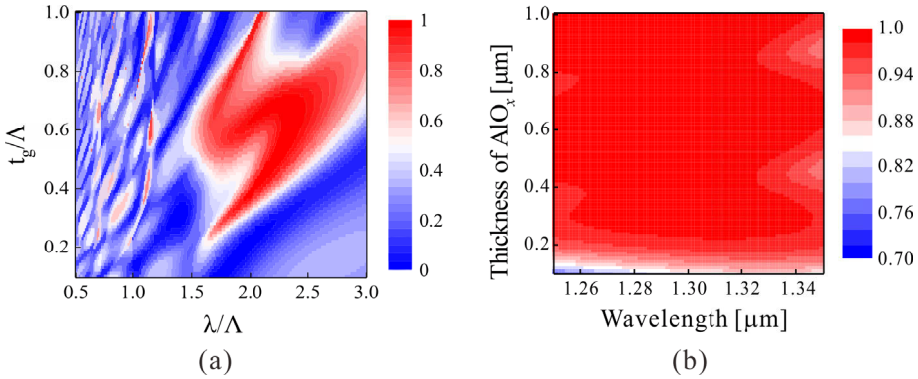

Fig. 2. (a) Reflectivity contour of the HCG as a function of normalized thickness (t_g/Λ) and normalized wavelength (λ/Λ) under normal incidence at DC = 0.55. (b) Reflectivity contour of the HCG as a function of wavelength and thickness of the AlO_x layer.

The fabrication of the HCG is similar to that in [33] and shown in Fig. 3. A Si_3N_4 layer is first deposited on the wafer by plasma-enhanced chemical vapor deposition (PECVD). PMMA electron resist is put on the top and then electron beam lithography (EBL) is used for defining the grating pattern. After development, the grating pattern is transferred to the Si_3N_4 layer by reactive ion etching (RIE) with a gas mixture of CHF_3/O_2. The grating structure is then transferred to the GaAs layer with the patterned Si_3N_4 layer as the mask by inductively coupled plasma (ICP) etching with a gas mixture of $Cl_2/BCl_3/Ar$. Then the wafer is loaded to the wet oxidation furnace. The $Al_{0.9}Ga_{0.1}As$ layer beneath GaAs layer is oxidized at 420 degrees by the water vapor flowing through the air gaps of the HCG. The oxidation rate is isotropic for $Al_{0.9}Ga_{0.1}As$ [34] and about 3 nm/min for the test structure. The SEM images of the cross section of the test structure and of the HCG are shown in Fig. 4 and Fig. 1(b), respectively. In Fig. 4, we can find that compared with the unpatterned GaAs region the GaAs-based bars in the patterned region shifts down by 21 nm after oxidation, which is caused by the layer contraction. Thus, we conclude that there is a 4.9% layer contraction for $Al_{0.9}Ga_{0.1}As$ layer after wet oxidation. Thus, the layer contraction of $Al_{0.9}Ga_{0.1}As$ is much smaller than that of $Al_{0.98}Ga_{0.02}As$ after wet oxidation [31], resulting in a more stable AlO_x layer. The HCG has a high fabrication tolerance. The simulation results show

OSA CONTINUUM

that the reflectivity of the HCG at 1300-nm range is enhanced slightly when the $Al_{0.9}Ga_{0.1}As$ layer is partly etched as shown in Fig. 4.

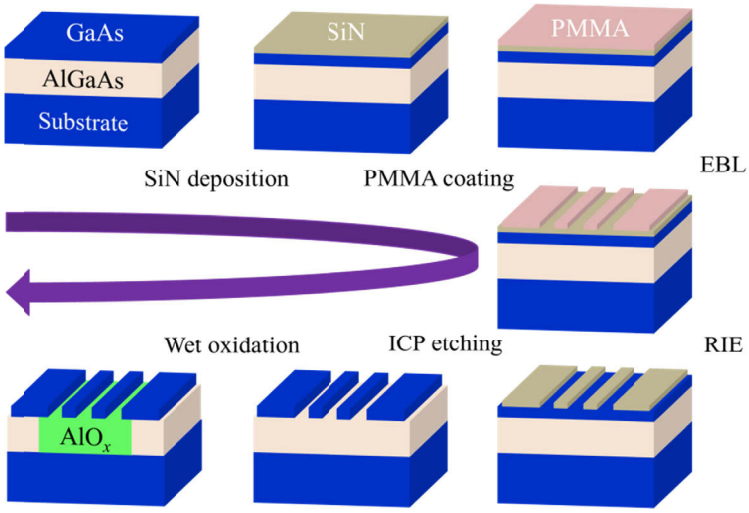

Fig. 3. Schematic of fabrication process of the HCG. PMMA, poly methyl methacrylate; EBL, electron beam lithography; RIE, reactive ion etching; ICP, inductively coupled plasma.

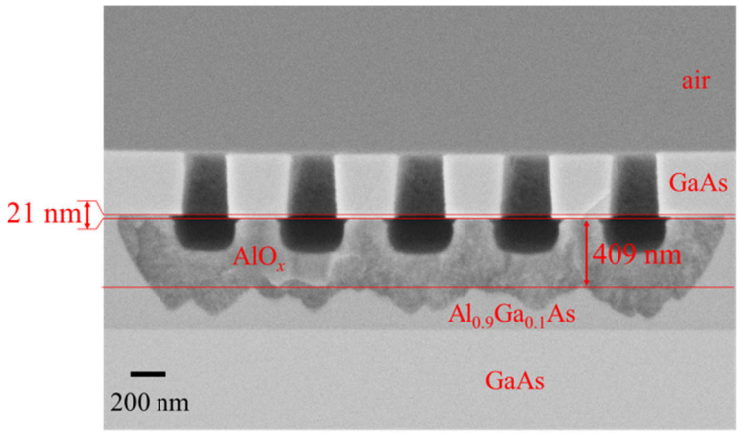

Fig. 4. SEM image of the cross section of a test structure for measuring the layer contraction and oxidation rate.

3. Results and discussions

The reflectivity spectrum of the HCG is measured with the setup reported in [33]. The broadband amplified spontaneous emission (ASE) (1270-1330 nm) from a praseodymium-doped fiber amplifier (PDFA) is collected by a fiber and then collimated by a lens. A Glan-Thomson polarizer polarizes the light. Finally, the light is focused on the HCG by an objective lens with 50× magnification and numerical aperture (NA) of 0.45. The reflected light is collected by another fiber via a planar beam splitter and then measured by an optical spectrum analyzer (OSA). The reflected light is partly led by a cube beam splitter into a charge-coupled device (CCD) camera to observe the position of the HCG. The reflectivity of a gold-coated mirror is measured for

OSA CONTINUUM

a reference. The reflectivity of the HCG is normalized to the reflectivity of the gold-coated mirror. The measured reflectivity spectrum of the HCG is shown in Fig. 5. The measured reflectivity of the processed HCG agrees well with the simulated reflectivity spectrum calculated by two-dimensional finite difference time domain (2D-FDTD) method for the finite-size HCG. The discrepancy between the simulated reflectivity spectrum and the measured result arises from the angular components of the focused incident beam with a finite size [35].

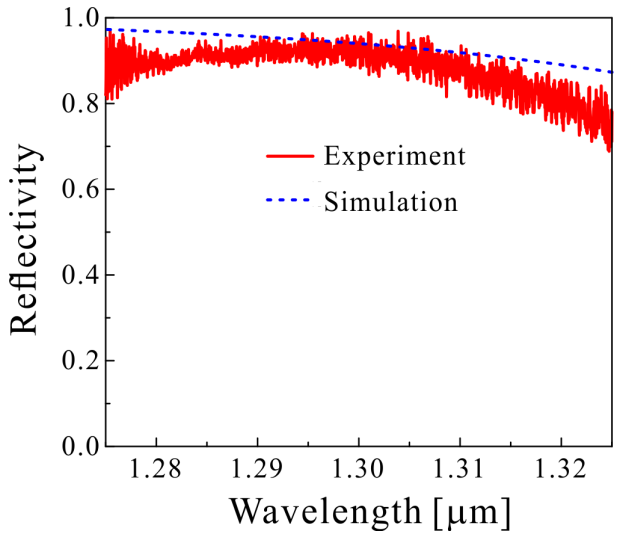

Fig. 5. Simulated and experimental results of the HCG (the measured width of the HCG bars is $a = 290$ nm). The simulated reflectivity spectrum is calculated by the 2D-FDTD method for a finite-size HCG.

In the measurement, the incident beam at normal incidence is a finite-size and focused beam and consists of a lot of angular components (i.e. a spread of wave-vector k points) after the objective lens. The angular components of the incident beam shape the reflectivity spectrum of the HCG, because the reflectivity of the HCG depends on the incident angle [33,35]. As an approximation, the average parallel wave-vector of the mode excited by a finite-size incident beam is inversely proportional to the lateral size of the incident beam, $k_{\parallel \mathrm{mod}} \propto \frac{1}{L}$, where L is the lateral size of the incident wave. The focused incident beam after the objective lens (NA: 0.45) has a divergence angle, also resulting in a spread of wave-vector k points. The average parallel wave-vector of the incident beam is proportional to the divergence angle of the incident beam, $k_{\parallel \mathrm{source}} \propto \theta$, where θ is the divergence angle of the incident beam [36,37]. Figure 6 shows the reflectivity spectra of the HCG under different incident angles (φ) and angular dependence of the HCG reflectivity. As the incident angle increases, the maximum reflectivity shifts to the longer wavelength side. The reflectivity at the shorter wavelength side is reduced, and the reflectivity at the longer wavelength side is increased. The reflectivity is sensitive to the incident angle [38]. The reflectivity is increased and then reduced when the incident angle varies from 0 degree to 30 degrees. In our experiments, the finite-size and focused incident beam can be considered as a sum of plane incident waves with different incident angles (i.e. higher-order angular components). The measured reflectivity of the HCG can be approximately expressed by $R = \int F^2(\varphi, \lambda) R(\varphi) d\varphi$, where $F(\varphi, \lambda)$, φ, and $R(\varphi)$ are the angular spectrum, the incident angle, and the angle-dependent reflectivity for a plane wave, respectively [39]. The higher-order angular components in the incident beam in the experiment and the imperfect sidewalls of the HCG may contribute to the discrepancy between the simulated reflectivity spectrum and the measured result, shown in Fig. 5.

OSA CONTINUUM

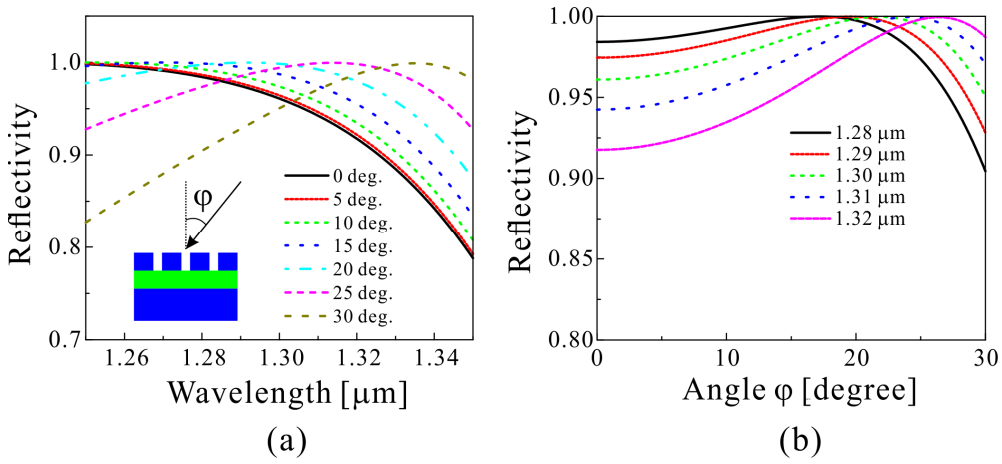

Fig. 6. (a) Reflectivity spectra of the HCG with plane incident waves with different incident angles (φ); (b) angular dependence of HCG reflectivity for plane incident waves.

4. Conclusions

GaAs-based HCG reflectors with AlO_x layer as the low-index medium oxidized from a 640-nm $Al_{0.9}Ga_{0.1}As$ layer were fabricated and measured. The HCG exhibits a reflectivity around 90% across the 1300-nm wavelength range, consistent well the simulation result. The layer contraction of the $Al_{0.9}Ga_{0.1}As$ layer is 4.9%, much smaller than that of the $Al_{0.98}Ga_{0.02}As$ layer after wet oxidation, resulting in a more stable AlO_x layer for real devices. In the fabrication of the HCG-VCSEL, the realization of the AlO_x layer oxidized from the $Al_{0.9}Ga_{0.1}As$ layer beneath the top patterned GaAs layer can be made simultaneously when the oxide aperture is formed. This HCG can be used in novel vertical cavities for narrow-linewidth VCSELs and for studies of fundamental physics like cavity quantum electrodynamics and cavity polaritons [40].

Funding

National Natural Science Foundation of China (61675193).

Disclosures

The authors declare no conflicts of interest.

References

1. F. Koyama, "Recent advances of VCSEL photonics," J. Lightwave Technol. **24**(12), 4502–4513 (2006).
2. R. Michalzik, "VCSELs - fundamentals, technology and applications of vertical-cavity surface-emitting lasers," Springer Series in Optical Sciences, **166** (2013).
3. A. Liu, P. Wolf, J. A. Lott, and D. Bimberg, "Vertical-cavity surface-emitting lasers for data communication and sensing," Photonics Res. **7**(2), 121–136 (2019).
4. A. Larsson, "Advances in VCSELs for communication and sensing," IEEE J. Sel. Top. Quantum Electron. **17**(6), 1552–1567 (2011).
5. H. Moench, S. Gronenborn, X. Gu, R. Gudde, M. Herper, J. Kolb, M. Miller, M. Smeets, and A. Weigl, "VCSELs in short-pulse operation for time-of-flight applications," Proc. SPIE **10938**, 109380E (2019).
6. L. A. Graham, H. Chen, J. Cruel, J. Guenter, B. Hawkins, B. Hawthorne, D. Q. Kelly, A. Melgar, M. Martinez, E. Shaw, and J. A. Tatum, "High power VCSEL arrays for consumer electronics," Proc. SPIE **9381**, 93810A (2015).
7. D. Budker and M. Romalis, "Optical magnetometry," Nat. Phys. **3**(4), 227–234 (2007).
8. P. M. Seiler, G. Ronniger, U. Troppenz, A. Sigmund, M. Moehrle, A. Peczek, and L. Zimmermann, "Novel concept for VCSEL enhanced silicon photonic coherent transceiver," AIP Adv. **9**(10), 105114 (2019).
9. S. Knappe, V. Shah, P. D. D. Schwindt, L. Hollberg, J. Kitching, L.-A. Liew, and J. Moreland, "A microfabricated atomic clock," Appl. Phys. Lett. **85**(9), 1460–1462 (2004).

OSA CONTINUUM

10. D. Kasahara, D. Morita, T. Kosugi, K. Nakagawa, J. Kawamata, Y. Higuchi, H. Matsumura, and T. Mukai, "Demonstration of blue and green GaN-based vertical-cavity surface-emitting lasers by current injection at room temperature," Appl. Phys. Express **4**(7), 072103 (2011).
11. M.-C. Amann and W. Hofmann, "InP-based long-wavelength VCSELs and VCSEL Arrays," IEEE J. Sel. Top. Quantum Electron. **15**(3), 861–868 (2009).
12. V. Karagodsky, F. G. Sedgwick, and C. J. Chang-Hasnain, "Theoretical analysis of subwavelength high contrast grating reflectors," Opt. Express **18**(16), 16973–16988 (2010).
13. R. Magnusson and M. Shokooh-Saremi, "Physical basis for wideband resonant reflectors," Opt. Express **16**(5), 3456–3462 (2008).
14. P. Debernardi, R. Orta, T. Gründl, and M.-C. Amann, "3-D vectorial optical model for high-contrast grating vertical-cavity surface-emitting lasers," IEEE J. Quantum Electron. **49**(2), 137–145 (2013).
15. A. Liu, W. Hofmann, and D. Bimberg, "2D analysis of finite size high-contrast gratings for applications in VCSELs," Opt. Express **22**(10), 11804–11811 (2014).
16. D. Fattal, J. Li, Z. Peng, M. Fiorentino, and R. G. Beausoleil, "Flat dielectric grating reflectors with focusing abilities," Nat. Photonics **4**(7), 466–470 (2010).
17. T.-C. Chang, K.-B. Hong, S.-Y. Kuo, and T.-C. Lu, "Demonstration of polarization control GaN-based micro-cavity lasers using a rigid high-contrast grating reflector," Sci. Rep. **9**(1), 13055 (2019).
18. M. C. Y. Huang, Y. Zhou, and C. J. Chang-Hasnain, "A surface-emitting laser incorporating a high-index-contrast subwavelength grating," Nat. Photonics **1**(2), 119–122 (2007).
19. E. Haglund, J. S. Gustavsson, J. Bengtsson, Å Haglund, A. Larsson, D. Fattal, W. Sorin, and M. Tan, "Demonstration of post-growth wavelength setting of VCSELs using high-contrast gratings," Opt. Express **24**(3), 1999–2005 (2016).
20. M. Gebski, M. Dems, J. Chen, Q. Wang, D. H. Zhang, and T. Czyszanowski, "Optical properties of GaAs/AlO_x and Si/SiO_x high contrast gratings designed for 980-nm VCSELs," IEEE Trans. Nanotechnol. **13**(3), 418–424 (2014).
21. S. Inoue, J. Kashino, A. Matsutani, H. Ohtsuki, T. Miyashita, and F. Koyama, "Highly angular dependent high-contrast grating mirror and its application for transverse-mode control of VCSELs," Jpn. J. Appl. Phys. **53**(9), 090306 (2014).
22. T. Ansbæk, I.-S. Chung, E. S. Semenova, and K. Yvind, "2013-nm tunable monolithic high index contrast subwavelength grating VCSEL," IEEE Photonics Technol. Lett. **25**(4), 365–367 (2013).
23. K. Li, C. Chase, P. Qiao, and C. J. Chang-Hasnain, "Widely tunable 1060-nm VCSEL with high-contrast grating mirror," Opt. Express **25**(10), 11844–11854 (2017).
24. W. Zhou, D. Zhao, Y.-C. Shuai, H. Yang, S. Chuwongin, A. Chadha, J.-H. Seo, K. X. Wang, V. Liu, Z. Ma, and S. Fan, "Progress in 2D photonic crystal Fano resonance photonics," Prog. Quantum Electron. **38**(1), 1–74 (2014).
25. S. Boutami, B. Benbakir, J.-L. Leclercq, and P. Viktorovitch, "Compact and polarization controlled 1.55 μm vertical-cavity surface emitting laser using single-layer photonic crystal mirror," Appl. Phys. Lett. **91**(7), 071105 (2007).
26. J. Ferrara, W. Yang, L. Zhu, P. Qiao, and C. J. Chang-Hasnain, "Heterogeneously integrated long-wavelength VCSEL using silicon high contrast grating on an SOI substrate," Opt. Express **23**(3), 2512–2523 (2015).
27. G. Almuneau, M. Condé, O. Gauthier-Lafaye, V. Bardinal, and C. Fontaine, "High reflectivity monolithic sub-wavelength diffraction grating with GaAs/AlO_x stack," J. Opt. **13**(1), 015505 (2011).
28. W. Hofmann, C. Chase, M. Müller, Y. Rao, C. Grasse, G. Böhm, M.-C. Amann, and C. J. Chang-Hasnain, "Long-wavelength high-contrast grating vertical-cavity surface-emitting laser," IEEE Photonics J. **2**(3), 415–422 (2010).
29. I.-S. Chung, J. Mørk, P. Gilet, and A. Chelnokov, "Subwavelength grating-mirror VCSEL with a thin oxide gap," IEEE Photonics Technol. Lett. **20**(2), 105–107 (2008).
30. C. H. Henry, "Theory of the linewidth of semiconductor lasers," IEEE J. Quantum Electron. **18**(2), 259–264 (1982).
31. K. D. Choquette, K. M. Geib, C. I. H. Ashby, R. D. Twesten, O. Blum, H. Q. Hou, D. M. Follstaedt, B. E. Hammons, D. Mathes, and R. Hull, "Advances in selective wet oxidation of AlGaAs alloys," IEEE J. Sel. Top. Quantum Electron. **3**(3), 916–926 (1997).
32. R. D. Twesten, D. M. Follstaedt, K. D. Choquette, and R. P. Schneider Jr., "Microstructure of laterally oxidized $Al_xGa_{1-x}As$ layers in vertical-cavity lasers," Appl. Phys. Lett. **69**(1), 19–21 (1996).
33. A. Liu, P. Wolf, J.-H. Schulze, and D. Bimberg, "Fabrication and characterization of integrable GaAs-based high-contrast grating reflector and Fabry–Pérot filter array with GaInP sacrificial layer," IEEE Photonics J. **8**(1), 1 (2016).
34. K. D. Choquette, K. M. Geib, H. C. Chui, B. E. Hammons, H. Q. Hou, and T. J. Drummond, "Selective oxidation of buried AlGaAs versus AlAs layers," Appl. Phys. Lett. **69**(10), 1385–1387 (1996).
35. A. Liu, W. H. E. Hofmann, and D. H. Bimberg, "Integrated high-contrast-grating optical sensor using guided mode," IEEE J. Quantum Electron. **51**(1), 1–8 (2015).
36. C. W. Hsu, B. Zhen, J. Lee, S.-L. Chua, S. G. Johnson, J. D. Joannopoulos, and M. Soljačić, "Observation of trapped light within the radiation continuum," Nature **499**, 188–191 (2013).
37. Y. Horie, A. Arbabi, S. Han, and A. Faraon, "High resolution on-chip optical filter array based on double subwavelength grating reflectors," Opt. Express **23**(23), 29848–29854 (2015).
38. K. Li, Y. Rao, C. Chase, W. Yang, and C. J. Chang-Hasnain, "Monolithic high-contrast metastructure for beam-shaping VCSELs," Optica **5**(1), 10–13 (2018).

OSA CONTINUUM

39. D. W. Peters, S. A. Kemme, and G. R. Hadley, "Effect of finite grating, waveguide width, and end-facet geometry on resonant subwavelength grating reflectivity," J. Opt. Soc. Am. A **21**(6), 981–987 (2004).
40. B. Zhang, Z. Wang, S. Brodbeck, C. Schneider, M. Kamp, S. Höfling, and H. Deng, "Zero-dimensional polariton laser in a subwavelength grating-based vertical microcavity," Light: Sci. Appl. **3**(1), e135 (2014).